# Mass Transport and Flow Regimes in Centrifugal Partition Chromatography

**L. Marchal and J. Legrand**
Laboratoire de Génie des Procédés-Environnement-Agroalimentaire, Université de Nantes, 44602 Saint-Nazaire Cedex, France

**A. Foucault**
Laboratoire de Biotechnologie et Molécules Marines, IFREMER, 44311 Nantes Cedex 03, France

*Centrifugal partition chromatography (CPC) is a support-free liquid–liquid separation process that depends for efficiency on the behavior of the two liquid phases. Hydrodynamics of phases was studied according to flow rate and centrifugal acceleration, using a transparent column and a stroboscopic video system. For the heptane-methanol two-phase system, three main flow regimes — stuck film, oscillating sheet, and atomization — are observed, highlighting the coriolis acceleration effect as well as the influence of the column shape. Mass transport in the CPC column is modeled by a plug flow with axial dispersion and mass transfer with a stagnant volume. Model parameters (residence time, Péclet number, partition ratio, and mass-transfer coefficient) are fitted on solute residence-time distribution. Off-column dispersion is an important source of peak broadening in CPC, whereas its irregular geometry provides a plug flow for mobile phase. Importance of flow pattern on mass transfer is demonstrated. CPC interest for preparative applications is confirmed.*

## Introduction

Centrifugal partition chromatography (CPC) is a support-free liquid–liquid separation process. This chromatographic method is based on the Nernst's distribution law (Nernst, 1891), which states that a solute will be distributed between two partially miscible solvent layers at a constant and reproducible ratio, $K_D$, of its concentration in one phase to its concentration in the other. Under ideal conditions, $K_D$, the partition ratio, is independent of the solute concentration and of the presence of other solutes.

As there is no solid support, the stationary phase remains in the column owing to its geometry and to the density difference between the two phases. This column shape, thought up by Murayama et al. (1982), consists of a series of small volumes or cells, connected by ducts in cascade, and subjected to an important centrifugal acceleration field (Figure 1).

The liquid nature of both phases means that either of them can be used as the mobile phase, so two means of elution are possible. In descending mode (DM), the mobile phase is the more dense one, sometimes called the lower one. It enters the cells at their center, and then falls naturally through the stationary phase in the centrifugal direction (Figure 1). At the outlet of the cell (at the peripheral part), the effluent is pumped through the duct to the next cell. When only the mobile phase leaves the cell, equilibrium is reached. In ascending mode (AM), the mobile phase is the less dense one, sometimes called the upper one. It enters the cells at their periphery, and rises naturally through the stationary phase in the centripetal direction.

In both cases, the chromatographic process occurs in each cell, where the two phases are in contact. According to their affinities for the two phases, the components of an injected mixture in a CPC column have different retention times in the instrument, $t_R$ (Eq. 1), and then they leave the column separately

$$t_R = \frac{V_m}{Q} + K_D \frac{V_s}{Q} \tag{1}$$

and

$$V_c = V_m + V_s, \tag{2}$$

Correspondence concerning this article should be addressed to J. Legrand.

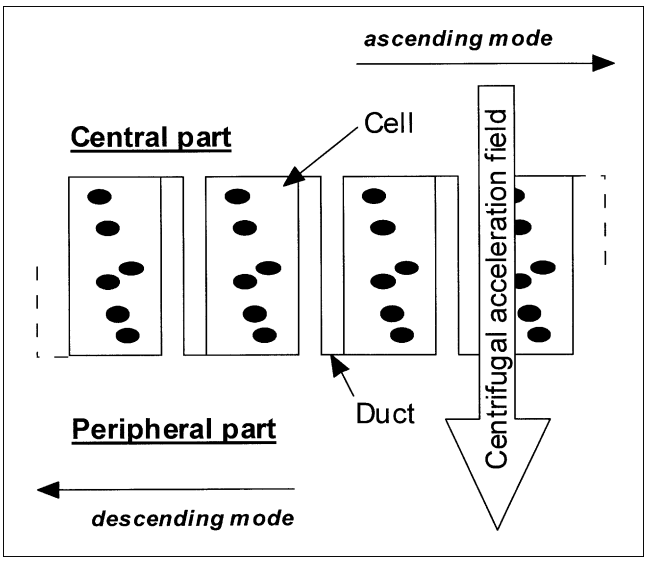


**Figure 1. CPC column, cells, ducts, and elution modes.**

Mobile phase is seen as dark ovals in the transparent stationary phase.

where $V_m$ is the mobile-phase volume, $V_s$ the stationary-phase one; $V_c$ the CPC column volume, and $Q$ the volumetric flow rate of the mobile phase. Different column geometry and cell fittings are commercially available (Foucault, 1995), but these instruments are still regarded as not being efficient, since more than 1000 theoretical plates are seldom encountered. Even if the two liquid phases can be finely tuned in order to give very selective systems, the separation of natural mixtures, often composed of homologs and analogs (Margraff, 1995), requires a more efficient apparatus.

When optimizing such a mass-transfer process, solvent selection, operating conditions, and design criteria need to be carefully evaluated. Murayama (1982) already showed that in CPC the resolution of a separation increases with the rotational speed and that it slightly decreases with the flow rate. They also observed that the amount of stationary phase retained in the column depends on the dynamic equilibrium of the two phases in each cell that is related to rotational speed, flow rate, and the solvent system properties. Models have been proposed to predict the phase volume ratio and the separation efficiency in CPC (Armstrong et al., 1988; Foucault et al., 1994). The mobile-phase flow behavior in the cells was considered successively as an emulsified band (Armstrong et al., 1988) and as single droplets (Foucault et al., 1994). It was then advisable to make flow visualization in CPC cells, in order to verify these assumptions and/or to permit column optimization. The pioneering visualizations in CPC were done thanks to van Halsema (1994) and van Buel et al. (1995, 1998) at the Kluyver Institute for Biotechnology of the Delft University of Technology. For phase visualization, they used dyes and a transparent CPC cartridge, the cell and duct dimensions being equal to that of the commercial CPC-LLN 250W cartridge (Sanki Eng. Ltd.). They showed the existence of four main flow regimes: droplets, jets, broken jets, and sprays. They specified then that visualization, pressure drop, and stationary-phase holdup are valuable tools for explaining separation efficiency, as well as for improving CPC columns.

Three input parameter groups acting on the liquid behavior in CPC can be considered: user parameters (flow rate, rotational speed, and elution mode), instrument parameters (cell and duct shape and material), and the two-phase system parameters (with the physical properties of the phases, such as, density, $\rho$, viscosity, $\eta$, and interfacial tension, $\gamma$). Parameters are summarized in Figure 2.

Flow regimes and mass transfer are of course interdependent aspects of CPC working. The more dispersed the mobile phase is, the more important the interfacial area and the volumetric mass transfer are. Phase ratio and pressure drop along the instrument are directly related to the phase equilibrium in each cell, and give additional information about the regime observed (Armstrong et al., 1998; van Buel et al., 1995). The first point to be considered is the relation between peak broadening and mass transfer in the cells. Martin and Synge (1941) proposed the theoretical plate model, which considers a chromatographic column as a series of stages in which the partition equilibrium between the two phases is instantaneously achieved. This model, which is still in current use in chromatographic science, does not permit investigation of the origin of broadening. In 1956, van Deemter et al. in-

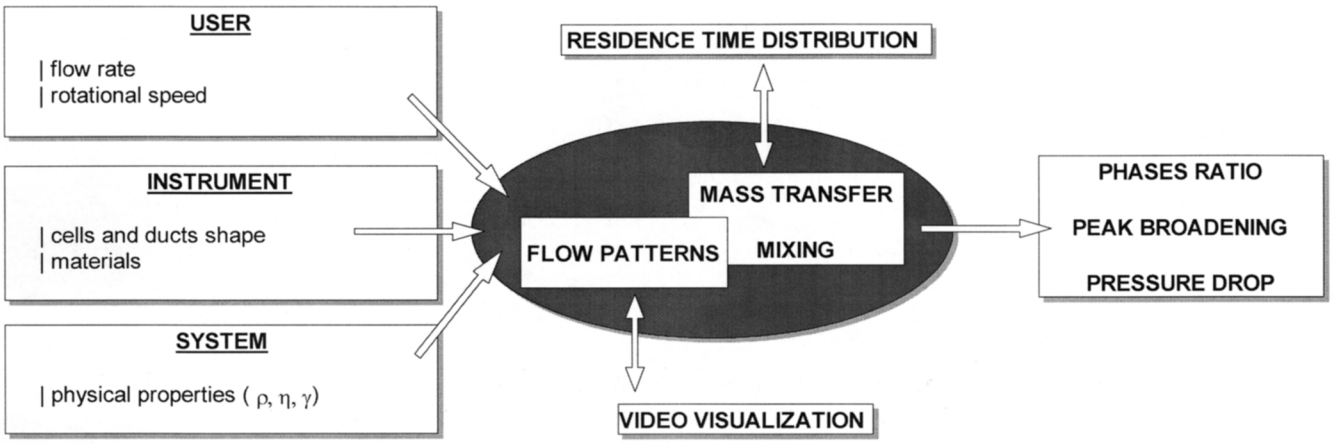


**Figure 2. Parameters in CPC.**

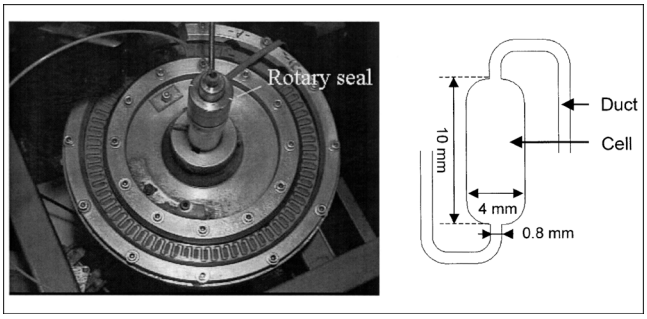


**Figure 3. Visual-CPC rotor on the left with a rotary seal joint and one cell on the right.**

troduced the notion of resistance to mass transfer in chromatography and its origins, such as longitudinal diffusion and finiteness of mass-transfer coefficient. The column is then considered to be a continuous medium with respect to the axial dimension. This model was generalized by Villermaux et al. (1992) for percolation processes, and applied to CPC by van Buel et al. (1997). Owing to the model parameters, it is now possible to locate the origin of band broadening in the column. The second point, not studied yet, concerns the influence of flow regimes on mass transfer.

Our first visualizations were basically made in order to optimize the column geometry by considering its influence on the flow patterns. In a preliminary work (Marchal et al., 2000), it was shown that for various two-phase systems, the increase of chromatographic efficiency always exists in a more dispersed flow regime. The interfacial area has an obvious influence, but mixing and interfacial renewal also have to be evaluated. The physical properties of the two-phase system, such as density difference, interfacial tension, or viscosity, have a large influence on the hydrodynamics phase in CPC. This will be treated in a later article.

Broadening the solute peak in this chromatographic setup may have different origins:

1. Injection method
2. Off-column setup (pipe fittings, valves, rotary seal joints)
3. Duct shape (mobile-phase flow)
4. Flow patterns in each cell (volumes and behavior of both phases).

**Table 1. Physical Properties of the Two-Phase System at 22°C (except $\gamma$, at 23°C)**

| $\rho$ UP $kg \cdot m^{-3}$ | $\rho$ LP $kg \cdot m^{-3}$ | $\Delta\rho$ $kg \cdot m^{-3}$ | $\gamma$ $10^{-3}$ $N \cdot m^{-1}$ | $\eta$ UP $10^{-3}$ Pa·s | $\eta$ LP $10^{-3}$ Pa·s |
|---|---|---|---|---|---|
| 684 | 756 | 72 | 1.16 | 0.47 | 0.65 |

As a result of these various contributions, elution peaks will be considered and modeled using a two-point measurement residence-time distribution (RTD) analysis for numerous operating conditions (rotational speed and flow rate). Flow patterns are visually (video) determined under the same conditions, owing to a stroboscopic system. The correlation between model and classic chromatographic parameters (number of theoretical plates and resolution) will be presented.

## Experimental Studies

A typical CPC instrument (like the HPCPC from Sanki Engineering Ltd., Kyoto, Japan, or the FCPC from Kromaton Technology, Angers, France) consists of polymer or metal disks engraved with cells and ducts, stacked in a rotor in series, and exposed to a constant centrifugal acceleration field produced by the rotation of this rotor around a fixed axis equipped with two rotary-seal joints for the inlet and outlet of the mobile phase (Figure 3).

The "visual CPC" is a CPC prototype designed to visualize the phase behavior in each cell. The visual CPC, the video instruments, and the chromatographic equipment were described in Marchal et al. (2000). The overall experimental setup is summarized in Figure 4.

As is often done in chromatography, the UV absorption property of solutes was used to determine the RTD.

### *Two-phase system and tracers*

One two-phase system, comprising two solvents, *n*-heptane and methanol (a well-known system for the separation of fatty acids and lipids), was used. Heptane and methanol were purchased from Carlo Erba (Rodano, Italy). The physical properties of each phase are summarized in Table 1. As heptane is partially miscible with methanol (miscibility of 30% w/w),

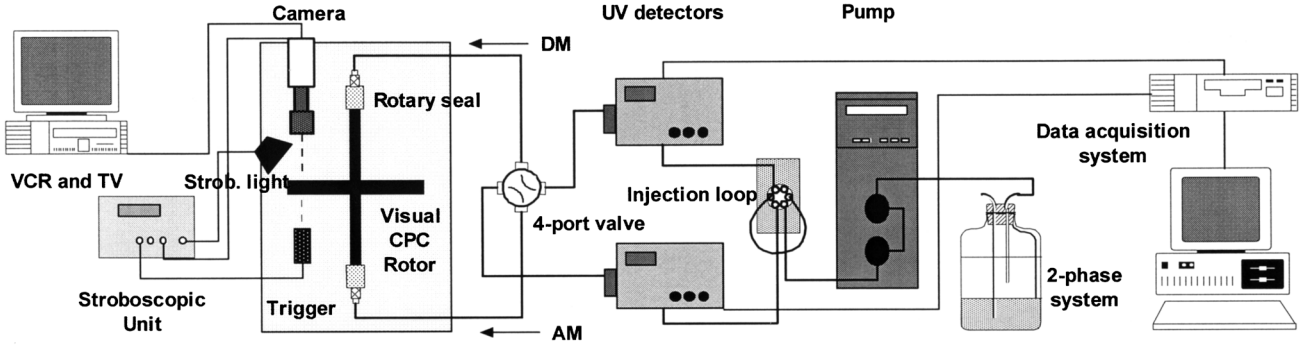


**Figure 4. Experimental setup: video equipment on the left, Visual-CPC in the middle, and injection-detection system on the right.**

the two mutually saturated phases have similar properties and low interfacial tension [measured at 23°C by Foucault et al. (1994) using the spinning-drop method]. The upper phase (UP) is heptane-rich, and the lower phase (LP) is methanol-rich. Viscosity was calculated by pressure-drop measurements in a 4-m capillary tube (Upchurch Scientific, Oak Harbor, WA, internal diameter of 0.254 mm), precalibrated with pure solvents. The method gives accurate results ($\pm 5\%$) according to values given in the literature (Robert, 1986). The densities of the saturated phases were measured by weighting a flask of given volume, calibrated with pure water at 22°C.

The study was done in the descending mode (LP is the mobile phase) for rotational speed values from 400 rpm up to 1500 rpm ($\pm 1$ rpm) and flow rates from 3 mL·min$^{-1}$ up to 24 mL·min$^{-1}$ ($\pm 0.1$ mL·min$^{-1}$). The *n*-heptane–methanol system was studied in both ascending and descending modes. The descending mode was chosen because it allowed us to obtain a larger number of flow regimes in the experimental domain investigated. Potassium nitrate ($KNO_3$) (R.P. Normapur from Prolabo, Paris, France) was used as a tracer for determining RTD in the mobile phase, because it has no affinity with heptane ($K_D = 0$). $KNO_3$ has a maximum UV absorption at 220 nm [the spectrum was achieved with a UV/Vis spectrometer (ATI UNICAM UV2 series spectrometer, Cambridge, UK)]. Phenyl salicylate (Sigma, St. Louis, MO, USA), used for determining the mass-transfer coefficients, has a partition ratio around 0.7 in DM and is detected at 280 nm.

### *Operating the visual CPC*

The temperature of the laboratory was fixed at 22°C ($\pm 0.5$°C) during all experiments. The two solvents, stocked at 22°C, too, were mechanically stirred together for a few minutes, which, after settling time, resulted in two perfectly saturated phases. Phases were combined in the flask, to be sure they are continuously equilibrated.

The following *modus operandi* is typical and often described (Armstrong et al., 1988; Foucault et al., 1992, 1994; van Buel et al., 1998). The four-port valve is set at the chosen mode position. The injection loop is filled with the sample in the mobile phase. The column is filled with the stationary-phase. The rotor is driven at the given rotational speed, and then the mobile phase elution is started at the given flow rate. The stationary-phase volume displaced during the equilibrium phenomenon is measured with a 25-mL graduated cylinder. If no more of the stationary-phase sample is taken out and if the UV detector's response is stabilized (constant and noiseless baseline), equilibrium is reached. The 6-port injection valve is put in the "inject" position and simultaneously data acquisition is started. When the solute elution is finished, acquisition is stopped, the injection valve is put in the "load" position and the column is refilled with the stationary-phase at rotational speed around 300 rpm. Video acquisition (15 s) is done during the solute elution.

## Model

The CPC column is divided into two parts: the off-column volume one and the chromatographic column one, and are occupied by both the mobile and stationary phases. The overall setup is shown in Figure 5. $V_c$ is the column volume, and $\epsilon_m = V_m/V_c$ is the mobile-phase fraction.

### *Assumptions*

Most of the assumptions of the model are those of the "ideal conditions" of the Nernst law. Since the solute concentration is low, that is, $K_D$ is constant in the linear part of the

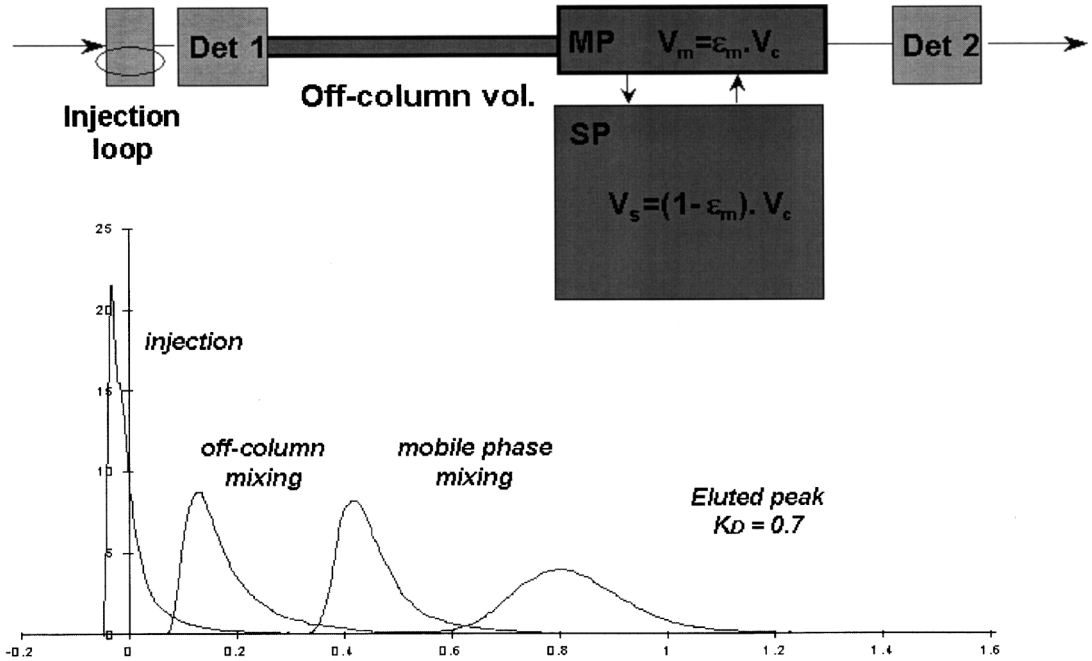


**Figure 5. CPC column considered in the model with various volumes and a peak deformation example.**

solubility isotherm. Moreover, van Buel et al. (1997), Berthod et al. (1992), Gluck and Martin (1990), and Armstrong et al. (1988) have already verified that retention of a solute in CPC is only due to partitioning (no adsorption).

It is assumed from two-layer interface model of Lewis and Whitman (1924) that mass transfer can be described by a linear driving-force model. If $C_m$ and $C_s$ are the concentrations of a solute in the mobile and stationary phases, respectively, the mass-transfer flux, $\Phi_M$, between both phases in a column element of the unit cross-section area and length $dz$ is

$$\Phi_M = k_0 a \cdot dz \cdot \left( C_m - \frac{C_s}{K_D} \right), \tag{3}$$

with $k_0$ ($\mathrm{m \cdot s^{-1}}$) the overall mass-transfer coefficient and $a$ ($\mathrm{m^2 \cdot m^{-3}}$) the specific interfacial area. Here $k_0$ can be expressed with regard to the mass-transfer coefficients in each phase ($k_m$ and $k_s$),

$$\frac{1}{k_0} = \frac{K_D}{k_m} + \frac{1}{k_s}. \tag{4}$$

### *Plug flow with axial dispersion model for off-column volume*

The mobile phase in the off-column volume is modeled by a plug flow with axial dispersion. The convection-diffusion equation for the concentration $C(z,t)$, is

$$U \frac{\partial C}{\partial z} + \frac{\partial C}{\partial t} = D_{\mathrm{ax}} \frac{\partial^2 C}{\partial z^2}, \tag{5}$$

with $U$ the linear velocity ($\mathrm{m \cdot s^{-1}}$) and $D_{\mathrm{ax}}$ the axial dispersion coefficient ($\mathrm{m^2 \cdot s^{-1}}$).

### *Plug flow with axial dispersion and mass exchange for column volume*

In the column, the mass transfer flux is superimposed on the purely convective flow and the axial dispersion flux of the previous model. For the mobile phase, it gives

$$\epsilon_m U \frac{\partial C_m}{\partial z} + \epsilon_m \frac{\partial C_m}{\partial t} + k_0 a \left( C_m - \frac{C_s}{K_D} \right) = \epsilon_m D_{\mathrm{ax}} \frac{\partial^2 C_m}{\partial z^2}, \tag{6}$$

and for the stationary phase

$$(1 - \epsilon_m) \frac{\partial C_s}{\partial t} - k_0 a \left( C_m - \frac{C_s}{K_D} \right) = 0 \tag{7}$$

Equation 7 is equivalent to

$$K_D C_m = T_m \frac{\partial C_s}{\partial t} + C_s, \tag{8}$$

where $T_m$ (s) is the mass-transfer time constant

$$T_m = \frac{K_D (1 - \epsilon_m)}{k_0 a}. \tag{9}$$

In the Laplace domain, where $L(C)$ is the Laplace transform of $C$, Eqs. 6 and 8 become

$$- D_{\mathrm{ax}} \frac{\partial^2 L(C_m)}{\partial z^2} + U \frac{\partial L(C_m)}{\partial z} + s \left( 1 + \frac{k'}{T_m s + 1} \right) L(C_m) = 0 \tag{10}$$

$$K_D L(C_m) = (T_m s + 1) L(C_s), \tag{11}$$

with $k' = K_D (1 - \epsilon_m)/\epsilon_m$, the retention factor.

The resolution of these equations leads to a transfer function $G(s)$, such as

$$L(C_m)(z = l) = G(s) L(C_m)(z = 0), \tag{12}$$

where

$$G(s) = \exp \frac{Pe}{2} \left( 1 - \sqrt{1 + \frac{4 t_0 s \left( 1 + \frac{k'}{T_m s + 1} \right)}{Pe}} \right), \tag{13}$$

where $Pe = (Ul/D_{\mathrm{ax}})$ is the Péclet number and $l$ is the column length: $l = t_0 U$.

### *Global CPC model*

The four parameters of the column model are:

$K_D$ = partition ratio

$t_0$ = mean residence time of a solute in the mobile phase

$Pe$ = mobile-phase Péclet number

$T_m$ = mass-transfer time constant

For the plug flow with the axial dispersion model (Eq. 5) for the off-column volume, the transfer function, $G_0(s)$, is equal to $G(s)$ when $T_m = 0$. This introduces two additional parameters:

The overall transfer function for the CPC setup is then:

$t_{\mathrm{off}}$ = mean residence time of a solute in the off-column volume

$Pe_{\mathrm{off}}$ = off-column Péclet number

The overall transfer function for the CPC setup is then:

$$G'(s) = G_0(s) \cdot G(s). \tag{14}$$

A computer program has been developed wherein both the injection and elution experimental curves are first normalized and then converted in Fourier series. Owing to the transfer function, the theoretical outlet curve is calculated from the injection curve and the model parameters are fitted, using the Rosenbrook algorithm, in order to minimize the difference (convergence criteria fixed at $10^{-8}$) between theoretical and experimental elution curves. Details on the method and the mathematics can be found in Legentilhomme et al. (1997).

### *Three-steps injection*

Six parameters cannot be fitted simultaneously without there being problems of model convergence. Each apparatus volume, off-column volume, and mobile phase and stationary

phase volumes will be considered successively. The two-point measurement method, with two detectors, permits no assumptions on the injection profile (type of impulsion and reproducibility). The axial dispersion due to the mobile phase flowing in the off-column volume is first estimated for each flow rate. The column is bypassed with a ZDV union [Upchurch (ZDV = zero dead volume)] between the inlet and the outlet tubes, and a first injection is done. Then $t_{off}$ and $Pe_{off}$ are fitted on the resulting RTD.

The column is equilibrated at the given operating conditions, and a solute with no affinity for the stationary phase, $KNO_3$, is injected. Then $t_0$ and $Pe$ are fitted on RTD, $t_{off}$ and $Pe_{off}$ are fixed at their previous values, and $T_m$ is fixed at 0.

Finally under the same conditions, a solute (phenyl salicylate), which separates in both phases is injected. RTD gives $K_D$ and $T_m$.

## Results and Discussion

First we present the observed flow regimes of both phases according to rotational speed and flow rate, then we will give and analyze the RTD and model fitting results with respect to the flow patterns.

### *Flow patterns*

In this part of the study, a description of the observed flow regimes is given and a flow chart of these regimes is made showing the operating conditions.

The injection of one liquid into another is important in many industrial operations. When mass transfer between two liquids has to be increased, the main way is to increase the dispersion of one liquid, that is, to convert the mobile phase into small droplets. The fundamental principle of destabilization of liquid is to increase the surface area of a sheet or a rod until it becomes unstable and disintegrates. Atomization processes have many technical solutions (Lefebvre, 1989) as pressure atomizers, twin-fluid ones, or rotary ones, but they cannot be applied in CPC cells. Simple geometrical solutions are possible as long as they come within the column manufacturing process possibilities. Then the objective is to design CPC cells in order to promote atomization phenomena of the mobile phase in the stationary one.

Due to interfacial tension phenomena, when two immiscible liquids are in contact, the interface area always tends to be minimized. In 1873, Plateau (1945) showed that a cylinder of liquid subjected to surface forces is unstable if its length exceeds its circumference, because it can be divided into spheres of equal volume with an accompanying decrease in surface area. This analysis indicated that surface forces are the cause of jet breakup. Since then, the theory of liquid surface instabilities has been widened to include a nonviscous liquid injected into a gas (Rayleigh, 1879), a viscous liquid injected into a gas (Weber, 1931), and one viscous liquid injected into another (Tomotika, 1935; Meister, 1967). It appears that the resulting flow behavior depends on the physical properties of liquid (viscosity and interfacial tension) and the flow characteristics in the injecting orifice. The mean velocity and the velocity profile (turbulent flat or fully developed parabolic) in the orifice are deciding factors (McCarthy et al., 1974; Ibrahim, 1997), as well as the wettability of the orifice material for expansion–contraction of the flow.

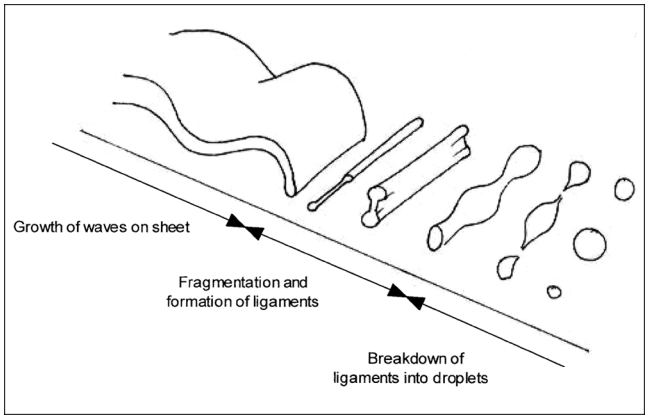


**Figure 6. Wavy disintegration mode of a liquid sheet.**

Three flow regimes for circular nozzles have been fully described in many works (Clift et al., 1978), according to the orifice velocity: first drops, then a jet that breaks up through axisymmetric amplification instabilities (Rayleigh instability), then the jet length increases before it decreases again due to asymmetric instabilities (waves), and when jet length is reduced to zero, atomization occurs. In CPC, the duct, whose cross-sectional dimensions are $0.8 \times 5$ mm, can be considered to be a "flat nozzle." Regimes for flat nozzles are quite different, and the mobile phase forms flat sheet instead of a jet. When the liquid sheet emerges from the nozzle, its development is influenced mainly by its initital velocity and liquid properties, like in the jet regime. Fraser and Eisenklam (1953) defined three modes of liquid-sheet destabilization in gas: rim, wave, and perforated-sheet. The rim mode occurs when both viscosity and interfacial tension are high. Surface forces then cause the free edge of the liquid sheet to contract into a thick rim, which then breaks up like a jet. In the perforated-sheet mode, holes appear in the sheet, delimited by rims formed by the liquid present inside. Holes grow rapidly until the rims of adjacent holes coalesce to produce ligaments that finally break up into nonuniform-size droplets. Wave motion can also appear (Figure 6), enlarge in the flow direction, leading to detached waves. As a result, these areas rapidly contract under the action of surface tension to form ligaments and then droplets.

In CPC, the mobile phase is pumped into the ducts, whereas centrifugal acceleration causes it to fall or settle in the cells. In the cell part, mobile-phase flow can be conceptually divided into three sequences: injection, free fall, and coalescence. The stroboscopic visualization allows us to see a cell as if we were on a rotating board. The observed flow paths are then considered in a rotating non-Galilean system. The resulting flow paths are submitted to two complementary accelerations that result from the composition law of acceleration (Coriolis, 1835): centrifugal acceleration, $\Gamma_c$, and coriolis acceleration, $\Gamma_{cor}$:

$$\Gamma_c = R_d \omega^2$$

$$\Gamma_{cor} = -2\,\mathbf{\Omega} \wedge V_R,$$

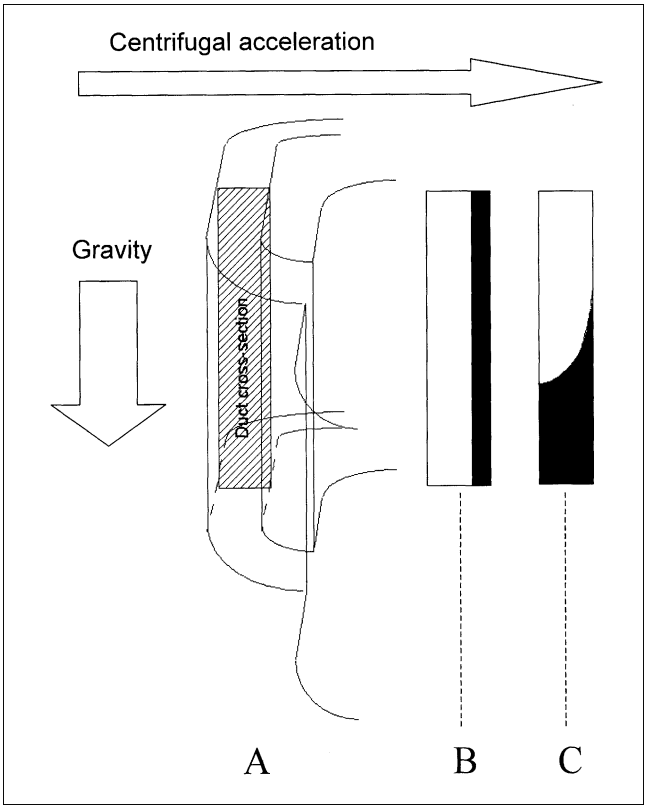


**Figure 7. Two-phase flow in the duct, at the entrance of the cell, according to gravity and centrifugal acceleration.**

(A) Sketch of the entrance part of a cell. The dashed area gives the cross-sectional area in the duct where the flow is considered. (B) Gravity is negligible, the mobile phase (dark colored) forms a film along the vertical wall of the duct. (C) Gravity is not negligible, the mobile phase flows in the lower part of the duct and a kind of meniscus is observed.

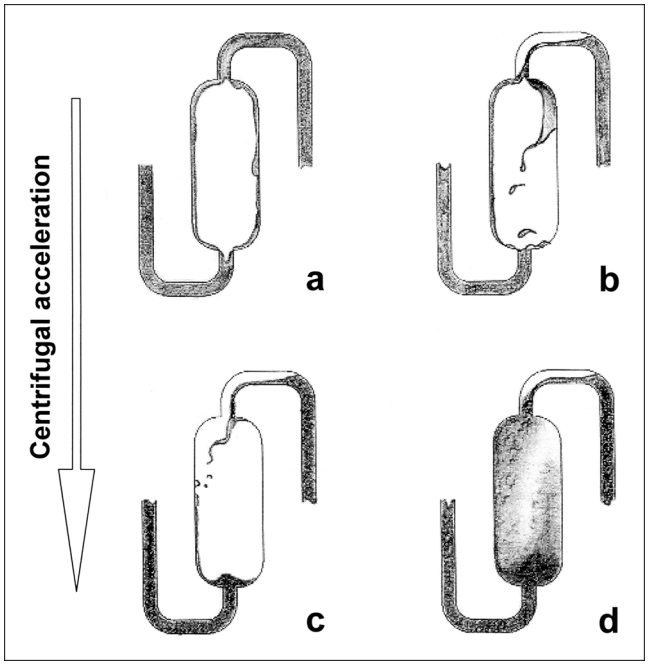


**Figure 8. Flow regimes in CPC according to video observations: (a) stuck film; (b) stuck film and oscillating sheet; (c) oscillating sheet; (d) atomization.**

where $R_d$ is the disk radius at the cell's center, $\omega$ is the angular velocity, $V_R$ is the relative velocity vector, and $\mathbf{\Omega}$ is the rotation vector.

Determination of the cell-injecting conditions is not obvious in CPC. As a result of the first visualizations, it appears that the duct is not perfectly wetted by mobile phase (van Buel et al., 1995). Part of stationary phase is forced into the duct. The same phenomenon is also observed with our apparatus. For rotational speeds greater than 700–900 rpm (56–93 $g$, where $g = 9.81$ m/s$^2$ is the gravitational acceleration value), a domain where the gravity becomes negligible, mobile phase spreads and forms a film in the nonradial part of the duct (the duct cross-sectional section with mobile and stationary phases locations is shown in Figure 7B). The film thickness depends on both rotational speed and flow rate. For lower rotational speed values (as gravity has an influence), a kind of meniscus is observed in the ducts; the mobile phase is then supposed to flow in the lower part of the duct with a certain degree of spreading along the duct's wall with respect to the centrifugal acceleration field (Figure 7C). In this case, wettability of the disk material and interfacial tension are expected to have a particular influence. Especially in descending mode, the mobile phase (methanol-rich phase) is a polar one, and so it leads to wetting of the steel surfaces.

Created during the injection, the interface shape is then correlated with the initial conditions and the hydrodynamics of both phases in the cells that are under the influence of external forces. Owing to the stroboscopic visualizations, three main flow regimes are observed:

1. Film adhering to the cell's side walls (Figure 8a);
2. Curvilinear sheet or film with oscillating instabilities (Figure 8c);
3. Atomization (Figure 8d).

No single droplets or emulsified bands were observed.

For each flow-rate value, at low centrifugal acceleration fields (400–700 rpm, that is, 18–56 $g$), the mobile phase flows as two films along the cell walls (Figure 8a). When the flow rate increases, one of the two films leaves the wall (Figure 8b). An increase in the rotational speed (700–900 rpm), causes a change in injection conditions and the two films become unstuck, resulting in a single oscillating or wavy sheet, which the coriolis force pushes away from the radial direction (Figure 8c). Some experiments are done in clockwise and counterclockwise rotation, and we can verify that the mobile-phase deviation is inverted as the coriolis force direction changes with the rotation direction (Figure 9). The sheet length decreases with increasing centrifugal acceleration, due to interfacial instabilities that are dependent on the sheet velocity, making droplets that are often too small to be distinguishable on the video screen. For lower flow rates, the sheet length decreases to zero, and a cloud of droplets is formed near the duct outlet. For higher flow rates ($Q \geq 15$ mL/min), instabilities appear on the mobile-phase film in the duct, causing a sudden atomization flow pattern (Figure 8d). Those favorable

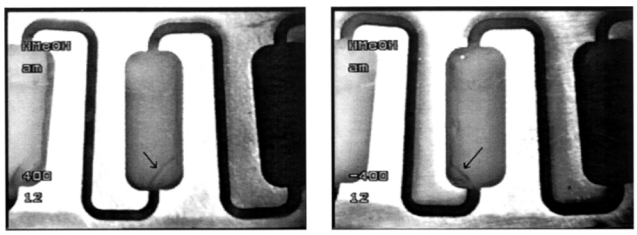

**Figure 9. Evidence of the coriolis acceleration effect: ascending mode, 400 rpm, 12 mL · min$^{-1}$, trigonometric rotation on the left and clockwise rotation on the right.**

instabilities linked to the flow-rate value result in the detachment of the mobile-phase film in the duct, perhaps due to the influence of coriolis acceleration and stationary phase flow structure. In spite of the coriolis force effect, in the atomization flow regime, the mobile phase is well distributed in all stationary phase volumes, and it can be assumed that strong recirculation flow occurs in the stationary-phase volume of the cell.

The flow chart of the flow regimes observed at each of the operating conditions is given in Figure 10, and shows the beneficial effects of both centrifugal acceleration and flow rate on the mobile-phase dispersion in the CPC cells. It must be emphasized that the flow chart was drawn for the heptane–methanol system, so it should be valid only for low viscosity, low density difference, and low interfacial tension systems.

Our observations of the two-phase behavior in the CPC cell confirm van Buel et al.'s previous studies, but they also supplement them. The influence of the injection type and cell-wall proximity are confirmed. Coriolis acceleration in the rotary system has a significant effect on the mobile-phase path deviation, as well as on instabilities, as its influence increases with velocity. Both centrifugal acceleration and flow rate apparently increase destabilization of film flow and mixing of the two phases in cells.

When there is poor phase separation or coalescence at the outlet of the cell, both phases exit the column, whereas only the mobile phase enters it. If the stationary-phase volume decreases in the column (a phenomenon that chromatographers call bleeding), the separation efficiency of the column will decrease, too. Equilibrium is reached when coalescence is complete, that is, when only the mobile phase leaves the cell. Coalescence depends on centrifugal acceleration, phase ratio, and stirring near the cell outlet.

### *Phases ratio*

Volumes of both phases in the model result from the hydrodynamic equilibrium in each cell, according to the flow regimes. Two methods are used to determine the different volumes: direct measurement with a graduated cylinder, and calculating the mean residence time of a one-phase flow at several flow rates. The two methods are in good agreement for both off-column and column volumes. The off-column volume, $V_{\text{off}} = 3.11$ mL $\pm 5\%$, and the column one, $V_c = 16.1$ mL $\pm 5\%$.

For the mobile phase, we use direct volume measurement and the mean residence time of potassium nitrate RTD. The two methods are also in good agreement, and show that there is no dead volume in the mobile phase. There is no obvious relation between the phases ratio and flow regimes within the experimental error, which may be due to the low number of cells in the studied column. The resulting mobile phase fraction, $\epsilon_m$, seems to be a linear increasing function of the flow rate, whereas it decreases with the acceleration field,

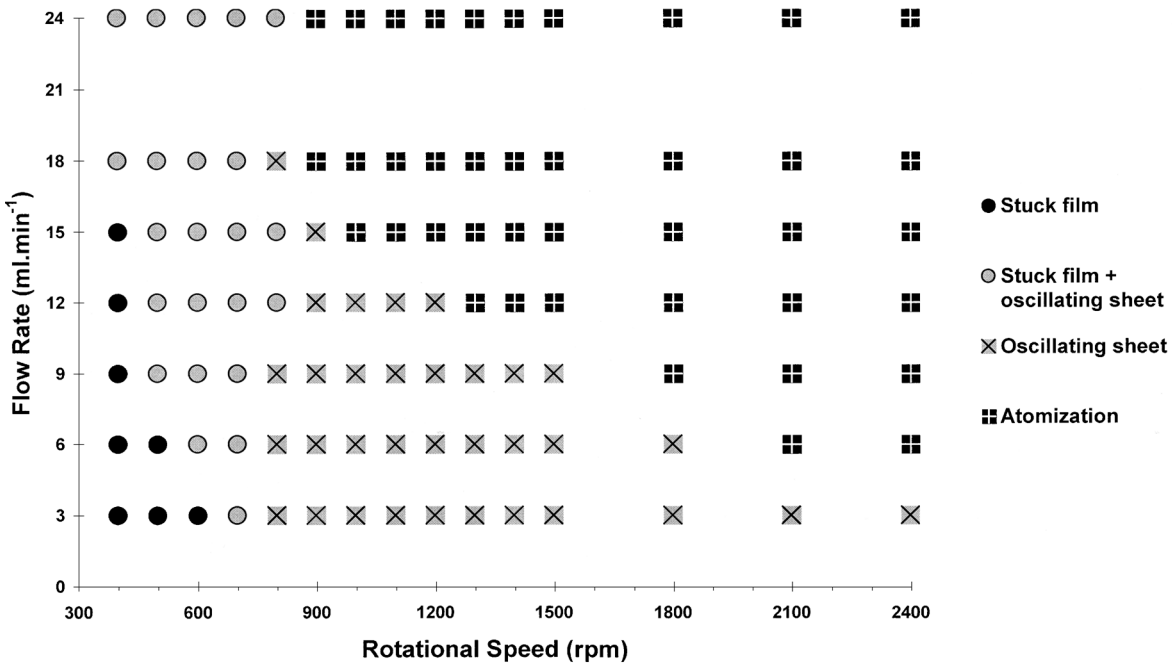


**Figure 10. Flow chart giving the observed flow regimes in the investigated experimental domain.**

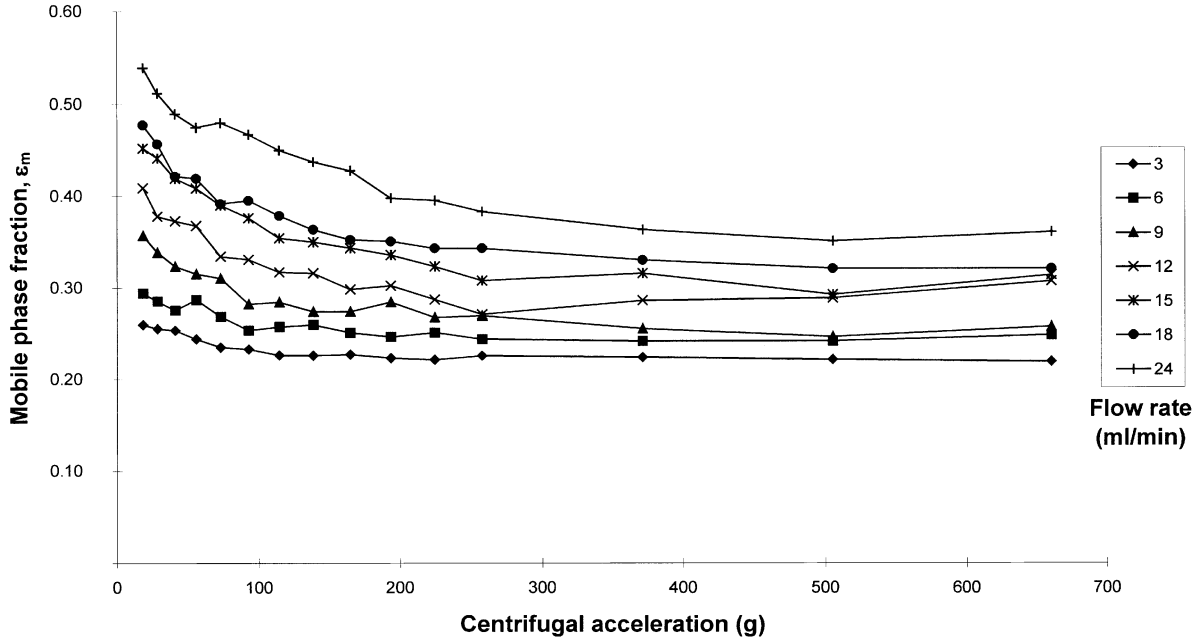


**Figure 11. Mobile phase fraction as a function of the centrifugal acceleration.**

reaching a minimum value (Figure 11). When $Q$ tends to 0, the $\epsilon_m$ value is the minimum of the mobile phase ratio available in the instrument, $\epsilon_{mo}$, which corresponds to the overall duct volume (Foucault et al., 1992), $\epsilon_{mo} = 0.20 \pm 5\%$. Here, 20% of the column volume does not participate in the separation step.

The mobile phase fraction, which evolves with the flow rate, has already been noted for this kind of two-phase system with other instruments (Foucault et al., 1992), and it seems to be representative of CPC working rather than related to CPC geometry. On the other hand, the decrease in $\epsilon_m$ with the acceleration value is quite new. At a given flow rate, the more dispersed the mobile phase is, the less important the mobile phase fraction. Both aspects, good dispersion and low $\epsilon_m$ values, enhance the column efficiency. The mobile-phase fraction is low even for high flow rates (less than 40% at 24 mL·min$^{-1}$). It thus can be assumed that higher flow rates can be used, which shows the potential interest of this geometry for preparative applications of CPC.

### *Axial dispersion*

Potassium nitrate RTD is also used to estimate the band broadening due to mobile phase flow in both off-column and the mobile phase part of the column volume.

The off-column volume (3.11 mL) consists mainly of a 1.016 mm ID (d) and a 382-cm-long peek tube (Upchurch, Oak Harbor, USA). The corresponding Reynolds number, $Re = (\rho Ud/\eta)$, varies from 70 to 600 with the flow rate, and is typical of a laminar flow. In Figure 12, the axial dispersion coefficient is plotted vs. the linear velocity $U$.

In established laminar flow in straight pipes, $D_{ax}$ is proportional to $U^2$ (Taylor, 1953). When $U$ is greater than 18 cm·s$^{-1}$, the law is not verified any more, and $D_{ax}$ reaches a limit value (around 400 cm$^2$/s). In the off-column setup, bends, valves, and joints create disturbances and diminish the laminar character of the flow. The values of $D_{ax}$ in the off-column volume setup will be kept constant, for given operating conditions, in the transfer function for further parameters for determining the CPC model in the column volume.

The values of the dispersion coefficients in the column volume are one hundred times lower than those obtained for the off-column volume. The model is fitted on the experimental curves with an error of less than 15%, showing that it is appropriate. There is no apparent influence of the mobile-phase fraction value on dispersion. Inside the column, straight ducts are very short. There is no stretch between two cells sufficiently long to have an established laminar flow. The axial dispersion coefficient is constant and negligible. In all cases, the mobile-phase flow behavior is close to that of a plug flow.

Off-column fittings are an important source of band broadening. Both the diameter and length of the tubing have to be reduced. The CPC column design characterized by tortuous ducts, sudden enlargements, and contractions provides a plug flow for the mobile phase for this low viscous phase system. Those results confirm that band broadening in CPC column is due only to mass-transfer limitation (van Buel et al., 1997), even if the duct geometry and flow regimes are different in both studies.

### *Mass transfer*

Determination of RTD with phenyl salicylate as a tracer is then used to find mass transfer. The previous parameters (average residence times and Péclet numbers in the mobile phase) are kept constant in transfer function, and both the partition ratio and mass-transfer constant time are fitted on phenyl salicylate RTD. First, $T_m$ is fitted with experimental curves and $K_D$ fixed at 0.7 (see Marchal et al., 2000). Both parameters are then found from previous values, with an average quadratic error of 4%. The resulting $K_D$ is a constant

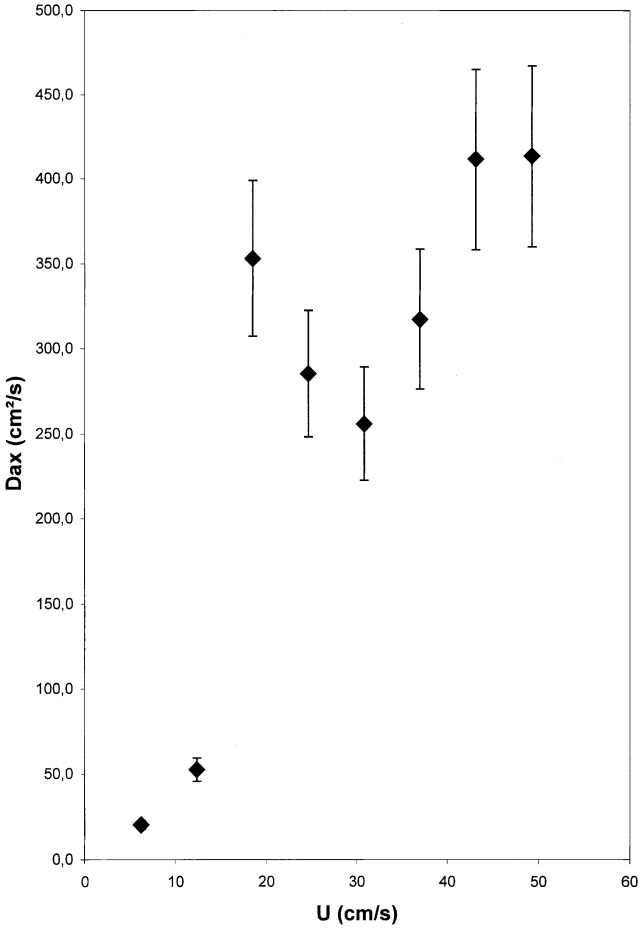


**Figure 12. Axial dispersion coefficient, as a function of linear velocity in the off-column volume.**

whose value is equal to $0.67 \pm 3\%$. The overall volumetric mass-transfer coefficients are calculated from $T_m$ values and presented in Figure 13 as a 2-D curve superimposed with the flow chart. Here, $k_0a$ varies from 0.02 $s^{-1}$ up to 2 $s^{-1}$. It

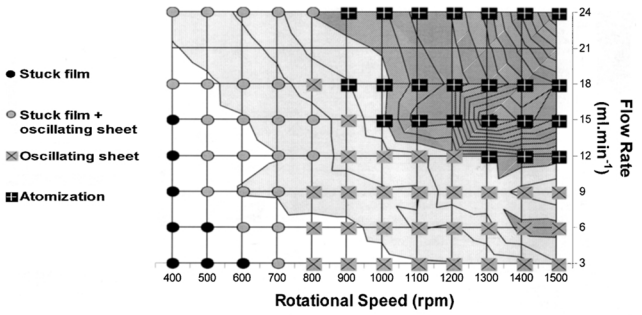


**Figure 13. Flow regimes and the overall volumetric mass-transfer coefficient ($s^{-1}$); evolutions with the flow rate and the rotational speed.**

$k_0a$ values: 0–0.1 $s^{-1}$, 0.1–0.4 $s^{-1}$, 0.4–1.8 $s^{-1}$. The horizontal lines are 0.1 $s^{-1}$ apart.

increases with both the rotational speed and flow rate, which agrees with the visual increase in the mobile phase dispersion and two-phase mixing. In fact, when part of the flow path spreads along the channel walls, $k_0a$ is quite low (0–0.2 $s^{-1}$). That corresponds to the low interfacial area between the two phases and the mobile phase at the wall contact. Those results are in the same range as that in van Buel et al. (1997) using Sanki instruments. This could be explained by the fact that the flow regimes observed by van Buel et al. correspond to the jets on the walls of the very thin cells (1.15 mm wide) of their apparatuses. Further information on the comparison between both systems can be found in Marchal et al. (2000). For a wavy or oscillating sheet regime, $k_0a$ varies between 0.1 and 0.5 $s^{-1}$, and within the experimental domain, centrifugal acceleration seems to have more of an influence than flow rate on the $k_0a$ variations. Lastly, $k_0a$ values greater than 0.5 $s^{-1}$ correspond to the atomization regime. The injection conditions in the transition zone, between 12 and 15 $mL \cdot min^{-1}$, makes $k_0a$ increase very rapidly (from 0.4 $s^{-1}$ up to 1.2 $s^{-1}$). For flow rates greater than 15 $mL \cdot min^{-1}$, $k_0a$ depends mainly on centrifugal acceleration, that is, specific interfacial areas do not increase with the flow rate in this regime. This confirms the Stokes' model (Foucault et al., 1994) that says that the mobile phase flows as droplets with diameters that depend only upon the acceleration value, while their number increases with the flow rate. For droplets, $a$ is proportional to $r^{-1}$ (if $r$ is their radius), and then $a$ does not depend on flow rate.

### *Efficiency and resolution*

$T_m$ is the ratio of the effective stationary-phase volume available for the solute to the overall mass-transfer coefficient. Let us define the retardation factor, $R$:

$$R = \frac{t_0}{t_R} = \frac{1}{1 + k'} \tag{15}$$

where the number of transfer units (NTU) is given by the ratio of the solute's residence time in the stationary phase and the mass transfer time constant:

$$NTU = \frac{t_R - t_0}{T_m} = (1 - R)\frac{t_R}{T_m}. \tag{16}$$

This depends on both mass-transfer kinetics and phase ratio in each cell. The height of a transfer unit (HTU) can be defined as the number of cells necessary to obtain a transfer unit:

$$HTU = N\text{cell}/NTU. \tag{17}$$

This characterizes the performance of one-cell geometry. Results for our system are presented on Figure 14. The behavior is the same for all flow rates within the experimental domain, and HTU decreases according to the centrifugal acceleration value, which leads to a limit value around unity. We can increase the flow rate up to this limit, and so diminish elution time, without any loss of separation efficiency, owing to the

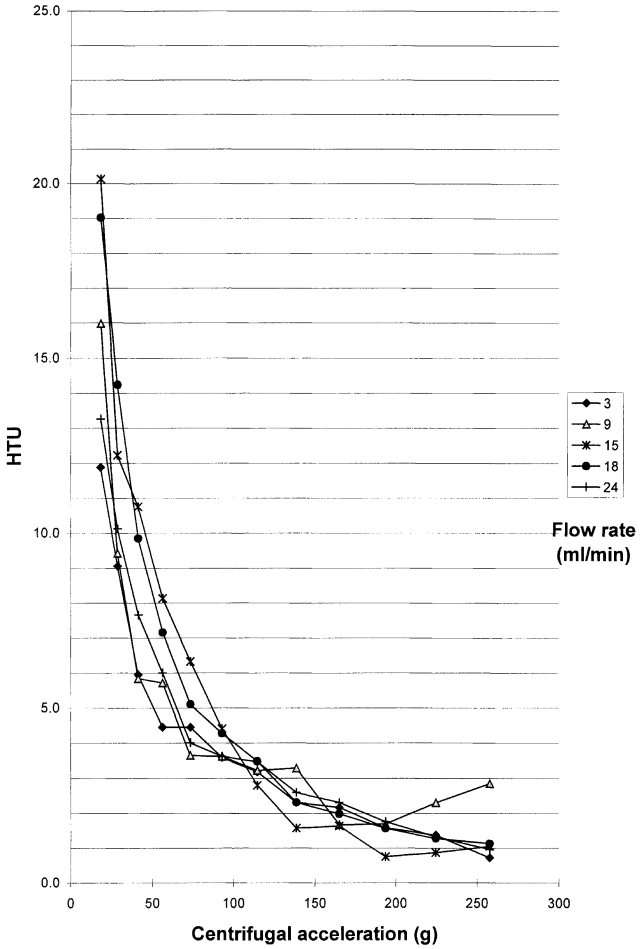


**Figure 14. Height of transfer unit as a function of the centrifugal acceleration.**

improvement in the overall transfer coefficient, even if the stationary-phase volume decreases.

By considering the transfer function, $G(s)$, of the column and the van der Laan relationship (Eq. 18) between the $k$-order momentum ($\mu_k$) of the impulse response of the system and its transfer function, we can calculate the mean retention time and the variance ($\sigma^2$) of a solute peak according to the parameters of the column model

$$\mu_i = (-1)^i \left[ \frac{\partial^i G}{\partial s^i} \right]_{(s=0)}, \tag{18}$$

so,

$$\frac{\sigma^2}{t_R^2} = \frac{2}{Pe} + \frac{2k'}{1+k'} \frac{T_m}{t_R}. \tag{19}$$

Because axial dispersion is negligible in the column volume,

$$\frac{\sigma^2}{t_R^2} = \frac{2k'}{1+k'} \frac{T_m}{t_R}. \tag{20}$$

Since the theoretical plate number is defined as follows:

$$N = \frac{t_R^2}{\sigma^2}, \tag{21}$$

the number of theoretical plates can be calculated as

$$N = \frac{1}{2} \left( \frac{1+k'}{k'} \right)^2 NTU. \tag{22}$$

Effective separation of peaks $A$ and $B$ is commonly expressed by the resolution $Rs$ defined for Gaussian peaks as

$$Rs = \frac{t_{RA} - t_{RB}}{2(\sigma_A + \sigma_B)}. \tag{23}$$

The approximate Knox equation (Purnell, 1960) gives an expression of resolution for two close Gaussian peaks (the separation factor, $\alpha$, which is equal to the ratio of the partition ratios of successive solutes, is close to one), according to chromatographic parameters

$$Rs = \frac{1}{4}(\alpha - 1)\sqrt{N} \frac{k'}{1+k'}. \tag{24}$$

Using Eq. 22, $Rs$ becomes

$$Rs = \frac{1}{4\sqrt{2}}(\alpha - 1)\sqrt{NTU}. \tag{25}$$

As an illustration of our results, a simulation has been carried out for $\alpha$ equal to 1.4 and for 20 disks of 66 cells (1320 cells and a column volume of 322 mL). Resolution appears to be a linear increasing function of centrifugal acceleration, whatever the flow-rate value. The 1.5 resolution value, commonly considered as sufficient to attain complete separation of the two successive peaks (baseline separation), is reached between 100 and 150 $g$. Using the apparent limit value of one transfer unit per cell, the baseline separation of solutes with this 20-disk instrument is still possible until a selectivity value of 1.23.

## Conclusion

We have demonstrated the importance of flow patterns in CPC. The relationship between the mass-transfer coefficient and flow regimes is linked to changes in a specific interfacial area. Centrifugal acceleration is the energy source for the mobile-phase atomization in CPC. A suitable nozzle can be defined as one cell entry that efficiently converts this energy to the liquid flow in order to destabilize it. The appearance of instabilities in the exit of the duct has a large effect on flow regimes and mass transfer. Three main flow regimes, which complement previous visualizations in CPC, are observed. The flow path is controlled both by wall proximity and centrifugal and coriolis accelerations. The atomization regime and recirculation in the stationary phase prevent the channeling problem often encountered in two-phase transfer processes. From an engineering point of view, the objective is to propose a suitable cell design in order to obtain atomization of the mobile phase, followed by a well-defined coalescence of the two phases in each cell. For a heptane–methanol

two-phase system, mobile phase fraction remains low within the experimental domain, and the coalescence step is efficient in the cells. The two-point measurement RTD and the proposed model are an accurate method for mass-transfer determination that proved to be extremely useful in our studies on improving the CPC process. Partitioning is described well and external sources of broadening are characterized, allowing us to study the column itself. The off-column setup is an important source of dispersion, and both the diameter and length of the tubing have to be reduced. The disk (cells and ducts) width does not favor axial dispersion apparition anymore, regardless of what the phase ratio and the flow regime are, owing to its geometry. Band broadening in the column itself is then only due to the limitations of mass transfer. Overall, the volumetric mass-transfer coefficient is used to characterize flow regimes, whereas the number of transfer units (NTU) is introduced to evaluate the separation process. NTU depends solely on centrifugal acceleration and no significant flow-rate effect is observed, which leads to one transfer unit per cell. Finally, the relationships between these parameters and classic chromatographic ones (theoretical plate number and resolution) are given. Further studies will focus on the effect of physical properties on the flow regimes and mass transfer of the two-phase system, and on some new column shapes designed in accordance with these results.

## Acknowledgments

G. Patissier from the Institute of Technology of the University of Nantes is thanked for carrying out the Visual CPC. J. M. Rosant and Y. Lorin from the Fluid Mechanics Laboratory of ECN (Central School of Nantes) are thanked for their helpful advice in flow visualization. This study was supported by Kromaton Technology (Angers, France), IFREMER (French National Research Institute for Exploitation of the Sea), and CNRS (French National Center for Scientific Research) in the framework of GIS PROGEBIO.

## Notation

$a$ = specific interfacial area
$AM, DM$ = ascending and descending mode
$C_m, C_s$ = concentrations in mobile and stationary phases
$D_{ax}$ = axial dispersion coefficient
$G, G_0$ = transfer functions of CPC column and off-column volume
$NTU, HTU$ = number and height of a transfer unit
$k_0, k_m$, and $k_s$ = overall and local mass-transfer coefficients
$k'$ = retention factor
$K_D$ = partition ratio
$l_{off}, l$ = off-column and column length
$N$ = theoretical plate number
$N_{cell}$ = cell number
$Pe, Pe_{off}$ = Péclet numbers, in the column and in the off-column volumes
$Q$ = volumetric flow rate
$R$ = retardation factor
$Re$ = Reynolds number
$Rs$ = resolution
$RTD$ = residence time distribution
$t_{off}$ = residence time in the off-column volume
$t_0$ = unretained solute residence time
$t_R$ = retention time
$T_m$ = mass-transfer time constant
$U$ = linear velocity
$V_{off}, V_c, V_m, V_s$ = off-column, column, mobile phase, and stationary phase volumes

### *Greek letters*

$\alpha$ = selectivity
$\epsilon_m$ = mobile phase fraction
$\gamma$ = interfacial tension
$\Gamma_c, \Gamma_{cor}$ = centrifugal and coriolis accelerations
$\eta_m, \eta_s$ = dynamic viscosities of mobile and stationary phases
$\rho_m, \rho_s, \Delta\rho$ = mobile and stationary phase densities, and the density difference

## Literature Cited

Armstrong, D. W., G. L. Bertrand, and A. Berthod, "Study of the Origin and Mechanism of Band Broadening and Pressure Drop in Centrifugal Countercurrent Chromatography," *Anal. Chem.*, **60**, 2513 (1988).

Berthod, A., R. A. Menges, and D. W. Armstrong, "Direct Octanol-Water Partition Coefficient Determination Using Co-Current Chromatography," *J. Liq. Chromatogr.*, **15**, 2769 (1992).

Clift, R., J. R. Grace, and M. E. Weber, *Bubbles, Drops, and Particles*, Academic Press, London (1978).

Coriolis, G. G., "Sur les Equations du Mouvement Relatif des Systèmes de Corps," *J. Ecole Roy. Polytech.*, **15**, 142 (1835).

Foucault, A. P., *Centrifugal Partition Chromatography*, Dekker, New York (1995).

Foucault, A. P., O. Bousquet, and F. Le Goffic, "Importance of the Parameter Vm/Vc in Countercurrent Chromatography: Tentative Comparison Between Intrument Designs," *J. Liq. Chromatogr.*, **15**, 2691 (1992).

Foucault, A. P., E. Camacho Frias, C. G. Bordier, and F. Le Goffic, "Centrifugal Partition Chromatography: Stability of Various Biphasic Systems and Pertinence of the 'Stokes Model' to Describe the Influence of the Centrifugal Field Upon the Efficiency," *J. Liq. Chromatogr.*, **17**, 1 (1994).

Fraser, R. P., and P. Eisenklam, "Research into the Performance of Atomizers for Liquids," *Imp. Coll. Chem. Eng. Soc. J.*, **7**, 52 (1953).

Gluck, S. J., and E. J. Martin, "Assessment of Centrifugal Partition Chromatography for Determination of Octanol-Water Partition Coefficients," *J. Liq. Chromatogr.*, **13**, 2529 (1990).

Ibrahim, E. A., "Effect of Velocity Profile on Liquid Sheet Instability," *Chem. Eng. Sci.*, **52**, 4419 (1997).

Lefebvre, A. H., *Atomization and Sprays*, Hemisphere, New York (1989).

Legentilhomme, P., L. Brujes, and J. Legrand, "Distribution of Staying Times of Liquid in a Non-Maintained Liquid-Solid Edding Flow: Influence of the Presence of Solids," *Chem. Eng. J.*, **67**, 83 (1997).

Lewis, W. K., and W. G. Whitman, "Principles of Gas Absorption," *Ind. Eng. Chem.*, **16**, 1215 (1924).

Marchal, L., A. Foucault, G. Patissier, J. M. Rosant, and J. Legrand, "Influence of Flow Patterns on Chromatographic Efficiency in Centrifugal Partition Chromatography," *J. Chromatogr. A*, **869**, 339 (2000).

Margraff, R., "Preparative Centrifugal Partition Chromatography," *Centrifugal Partition Chromatography*, A. P. Foucault, ed., Dekker, New York (1995).

Martin, A. J. P., and R. L. M. Synge, "A New Form of Chromatogram Employing Two Liquid Phases," *Biochem. J.*, **35**, 1358 (1941).

McCarthy, M. J., and N. A. Malloy, "Review of Stability of Liquid Jets and the Influence of Nozzle Design," *Chem. Eng. J.*, **7**, 1 (1974).

Meister, B. J., and G. F. Scheele, "Generalized Solution of the Tomotika Stability Analysis for a Cylindrical Jet," *AIChE J.*, **13**, 682 (1967).

Murayama, W., T. Kobayashi, Y. Kosuge, H. Yano, Y. Nunogaki, and K. Nunogaki, "A New Centrifugal Counter-Current Chromatograph and Its Application," *J. Chromatogr.*, **239**, 643 (1982).

Nernst, W., "Verteilung eines Stoffes zwischen zwei Lösungsmitteln und zwischen Lösungsmittel und Dampfraum," *Z. Phys. Chem.*, **8**, 110 (1891).

Plateau, J., "Statique Expérimentale et Théorique des Liquides Soumis aux seules Forces Moléculaires," *Theory of Sound*, J. S. Rayleigh, ed., Dover, New York (1945).

Purnell, J. H., "The Correlation of Separation Power and Efficiency of Gas-Chromatographic Columns," *J. Chem. Soc.*, 1268 (1960).

Rayleigh, J. S. W., "On the Instability of Jets," *Proc. London Math. Soc.*, **10**, 4 (1879).

Robert, C. W., *CRC Handbook of Chemistry and Physics*, CRC Press, Boca Raton, FL (1986).
Taylor, G., "Dispersion of Soluble Matter in Solvent Flowing Slowly Through a Tube," *Proc. Roy. Soc. A*, **219**, 186 (1953).
Tomotika, S., "On the Instability of a Cylindrical Thread of a Viscous Liquid Surrounded by Another Viscous Liquid," *Proc. Roy. Soc. A*, **150**, 322 (1935).
Van Buel, M. J., L. A. M. van der Wielen, and K. Ch. A. M. Luyben, "Pressure Drop in Centrifugal Partition Chromatography," *Centrifugal Partition Chromatography*, A. P. Foucault, ed., Dekker, New York (1995).
Van Buel, M. J., L. A. M. van der Wielen, and K. Ch. A. M. Luyben, "Effluent Concentration Profiles in Centrifugal Partition Chromatography," *AIChE J.*, **43**, 693 (1997).
Van Buel, M. J., F. E. D. van Halsema, L. A. M. van der Wielen, and K. Ch. A. M. Luyben, "Flow Regimes in Centrifugal Partition Chromatogtaphy," *AIChE J.*, **44**, 1356 (1998).
Van Deemer, J. J., F. J. Zuiderweg, and A. Klinkenberg, "Longitudinal Diffusion and Resistance to Mass Transfer as Causes of Nonideality in Chromatography," *Chem. Eng. Sci.*, **5**, 271 (1956).
Van Halsema, F. E. D., *Flow Regimes in Centrifugal Partition Chromatography*, MS Thesis, Delft University of Technology, Delft, The Netherlands (1994).
Villermaux, J., D. Schweich, and M. Sardin, "Modeling of Chromatographic Processes: A Chemical Engineering Approach," *Preparative and Production Scale Chromatography*, G. Ganetsos and P. E. Barker, eds., Dekker, New York (1992).
Weber, C., "Disintegration of Liquid Jets," *Z. Angew. Math. Mech.*, **11**, 136 (1931).

*Manuscript received June 21, 2001, and revision received Jan. 25, 2002.*